Inorganic Chemistry

Article

pubs.acs.org/IC

An Isomorphous Series of Cubic, Copper-Based Triazolyl Isophthalate MOFs: Linker Substitution and Adsorption Properties

Jörg Lincke,[†] Daniel Lässig,[†] Merten Kobalz,[†] Jens Bergmann,[†] Marcel Handke,[†] Jens Möllmer,[‡] Marcus Lange,[‡] Christian Roth,[†] Andreas Möller,[‡] Reiner Staudt,[§] and Harald Krautscheid*[,†]

[†]Fakultät für Chemie und Mineralogie, Universität Leipzig, Johannisallee 29, D-04103 Leipzig, Germany

[‡]Institut für Nichtklassische Chemie e.V., Permoserstraße 15, D-04318 Leipzig, Germany

[§]Fakultät Maschinenbau und Verfahrenstechnik, Hochschule Offenburg, Badstraße 24, D-77652 Offenburg, Germany

Supporting Information

ABSTRACT: An isomorphous series of 10 microporous copper-based metal−organic frameworks (MOFs) with the general formulas $^3_\infty[\{Cu_3(\mu_3\text{-}OH)(X)\}_4\{Cu_2(H_2O)_2\}_3(H\text{-}R\text{-}trz\text{-}ia)_{12}]$ (R = H, CH_3, Ph; X^{2-} = SO_4^{2-}, SeO_4^{2-}, 2 NO_3^{2-} (**1**−**8**)) and $^3_\infty[\{Cu_3(\mu_3\text{-}OH)(X)\}_8\{Cu_2(H_2O)_2\}_6(H\text{-}3py\text{-}trz\text{-}ia)_{24}Cu_6]X_3$ (R = 3py; X^{2-} = SO_4^{2-}, SeO_4^{2-} (**9**, **10**)) is presented together with the closely related compounds $^3_\infty[Cu_6(\mu_4\text{-}O)(\mu_3\text{-}OH)_2(H\text{-}Metrz\text{-}ia)_4][Cu(H_2O)_6](NO_3)_2{\cdot}10H_2O$ (**11**) and $^3_\infty[Cu_2(H\text{-}3py\text{-}trz\text{-}ia)_2(H_2O)_3]$ (**12**^{Cu}), which are obtained under similar reaction conditions. The porosity of the series of cubic MOFs with **twf-d** topology reaches up to 66%. While the diameters of the spherical pores remain unaffected, adsorption measurements show that the pore volume can be fine-tuned by the substituents of the triazolyl isophthalate ligand and choice of the respective copper salt, that is, copper sulfate, selenate, or nitrate.

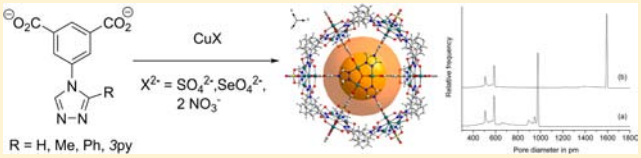

INTRODUCTION

In the last decades, metal−organic frameworks (MOFs) are an emerging class of porous solids.[1] Depending on their structure and porosity, they possess a high potential not only for applications in gas separation and storage,[2,3] but also in sensorics[4] and in heterogeneous catalysis.[5]

With the IRMOF series, Yaghi and co-workers have made significant contributions to a concept for a more rational design of MOFs.[6] In principle, the IRMOF concept represents an approach based on the connectivity of the fragments (e.g., SBU and ligand). A single MOF is then characterized by the connectivity of the ligand and the SBU and the resulting topology. As long as these preconditions are fulfilled by another set of ligands (and/or SBUs), it has to be expected from the IRMOF concept that a MOF of the same topology should exist. Within this frame, the pore size and shape are supposed to be determined by the choice of the ligand. Recently, Snurr et al.[7] have presented a large-scale screening of hypothetical metal−organic frameworks, which represents the latest breakthrough in the IRMOF approach.

Besides pure carboxylate ligands, less investigated nitrogen-rich heterocycles such as imidazoles,[8] pyrazoles,[9] 1,2,4-triazoles,[10,11] and tetrazoles[11,12] exhibit a promising coordination chemistry for the synthesis of MOFs. In our work, we focused on the design of novel ligands combining neutral 1,2,4-triazole and anionic carboxylate groups, as these ligands have the following advantages: low overall charge, robustness against oxidizing agents, suitable coordination chemistry, and adjustable derivatization. Because of these properties, MOFs containing these ligands may find potential application in gas separation or catalysis. In case of the coordination polymer $^3_\infty[Cu(Me\text{-}4py\text{-}trz\text{-}ia)]$[13] (Me-4py-trz-ia^{2-}: 5-(3-methyl-5-(pyridin-4-yl)-4*H*-1,2,4-triazol-4-yl)isophthalate), we recently presented a study showing the applicability of this class of coordination polymers for the separation of methane from nitrogen.[14]

On the basis of four 3-substituted 1,2,4-triazolyl isophthalate ligands,[15] we herein present a series of 10 isomorphous copper MOFs **1**−**10** (Table 1). The substituents, hydrogen, methyl, phenyl, and 3-pyridyl, differ in their steric demand as well as in

Table 1. Summary of the MOF Series $^3_\infty[\{Cu_3(\mu_3\text{-}OH)(X)\}_4\{Cu_2(H_2O)_2\}_3(H\text{-}R\text{-}trz\text{-}ia)_{12}]$ (1−8) and $^3_\infty[\{Cu_3(\mu_3\text{-}OH)(X)\}_8\{Cu_2(H_2O)_2\}_6(H\text{-}3py\text{-}trz\text{-}ia)_{24}Cu_6X_3]$ (9, 10)

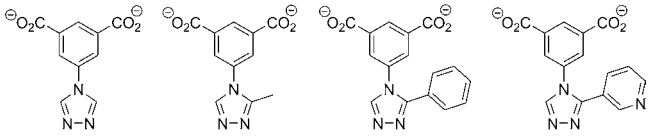

(trz-ia)$^{2-}$ (H-Me-trz-ia)$^{2-}$ (H-Ph-trz-ia)$^{2-}$ (H-3py-trz-ia)$^{2-}$

	R	X^{2-}		R	X^{2-}
1	H	SO_4^{2-}	**6**	Ph	SO_4^{2-}
2	H	SeO_4^{2-}	**7**	Ph	SeO_4^{2-}
3	H	$2NO_3^-$	**8**	Ph	$2NO_3^-$
4	Me	SO_4^{2-}	**9**	3py	SO_4^{2-}
5	Me	SeO_4^{2-}	**10**	3py	SeO_4^{2-}

Received: February 13, 2012
Published: July 2, 2012

   dx.doi.org/10.1021/ic3003228 | *Inorg. Chem.* 2012, 51, 7579−7586

their electronic influence. Besides varying ligands, the presented MOFs are accessible with different counterions incorporated in the structure, sulfate, selenate, and nitrate. On the basis of the porous nature of these MOFs, comprehensive adsorption studies with different adsorptives were carried out to assess the influence of both kinds of variations on the adsorption properties.

$^3_\infty[\{Cu_3(\mu_3\text{-}OH)(X)\}_4\{Cu_2(H_2O)_2\}_3(H\text{-}R\text{-}trz\text{-}ia)_{12}]$ (1−8) AND $^3_\infty[\{Cu_3(\mu_3\text{-}OH)(X)\}_8Cu_2(H_2O)_2\}_6(H\text{-}3py\text{-}trz\text{-}ia)_{24}Cu_6]X_3$ (9 AND 10)

X-ray Crystallography. The crystal structures of 4 out of the 10 presented compounds were elucidated by X-ray diffraction. As

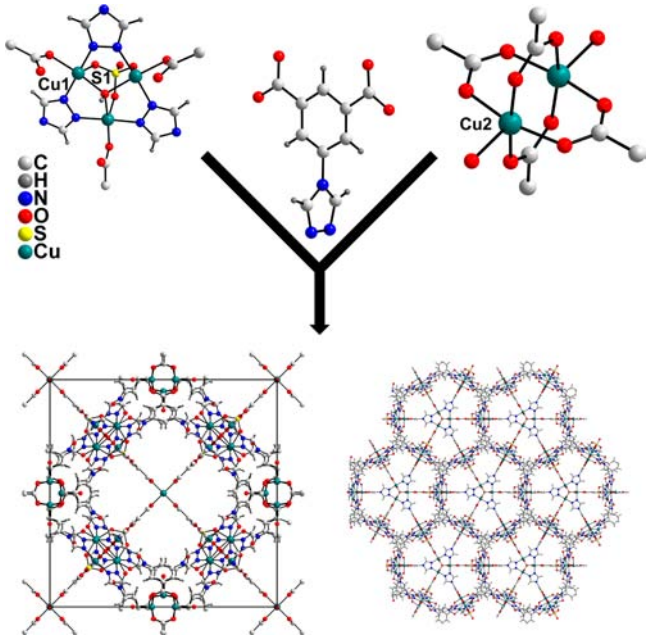

Figure 1. Fragments of the crystal structure of **1** (top, 50% ellipsoids), and view along [100] (bottom left) and [111] (bottom right).

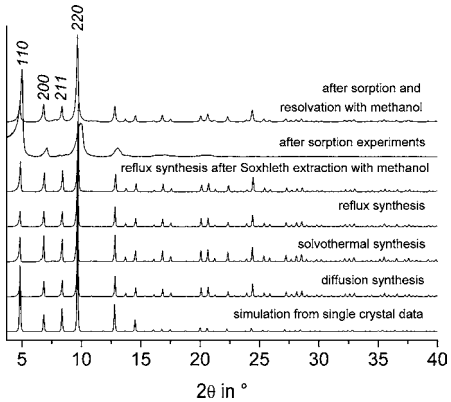

Figure 2. X-ray powder patterns (λ(Cu $K_{\alpha 1}$) = 154.060 pm) of **1** obtained by three synthetic methods, that is, diffusion, solvothermal, and reflux synthesis, together with the powder patterns after different postsynthetic treatments.

the single crystals of **10** were only weakly diffracting using conventional laboratory X-ray sources, synchrotron radiation was used to obtain a high-resolution data set. Representatively, the crystal structure of **1** is further discussed. Single crystals of **1** suitable for X-ray structure analysis were obtained by slow diffusion of solutions of $CuSO_4 \cdot 5H_2O$ and $(H_2NMe_2)H(trz\text{-}ia)$ in H_2O/MeCN (1:1, v/v). **1** crystallizes in the noncentrosymmetric cubic space group $I\bar{4}3m$ (No. 217) with two formula units per unit cell. The absolute structure parameter of 0.54(2) points to an inversion twinning. The crystal structure possesses two structural motifs (cf., Figure 1): a trinuclear hydroxy bridged copper unit and a paddle wheel unit. Both the sulfate ion and the hydroxy group, which reside on the 3-fold axis, bridge the three copper ions. The distorted square pyramidal N_2O_3-coordination of the corresponding copper ion (Cu1) is accomplished by monodentately binding carboxylates as well as by two bidentately bridging triazole units. The isophthalate group of the ligand resides on the mirror plane, whereas the triazole ring is oriented perpendicular. In contrast, the paddle wheel unit is located on two mirror planes (site symmetry 2*mm*). Selected bond lengths and angles of **1** are summarized in Table SI-2.

While the trinuclear hydroxy bridged copper unit represents a six-connected nodal point, the paddle wheel unit acts as four-connected nodal point. By linkage through the three-connecting $(trz\text{-}ia)^{2-}$ ligand, a three-dimensional framework of **twf-d** topology[16] with 66% solvent accessible pore volume[17] is built up. As shown in Figures 1 and 3, **1** possesses cage like pores. In total, the wall of a single cage consists of 6 paddle-wheel units, 8 $[Cu_3(\mu_3\text{-}OH)]^{5+}$, groups and 24 triazolyl isophthalate ions. To ensure phase purity, powder X-ray diffraction (PXRD) measurements were performed (Figure 2). By comparison of the experimental powder pattern with the pattern simulated from the single-crystal data, phase purity can be concluded.

Furthermore, **1** was not only synthesized by diffusion, but also by solvothermal synthesis and can be obtained in multigram scale as microcrystalline powder by heating the starting materials under reflux. The other compounds **2**−**10** can be obtained by one or more of these synthetic methods. Whereas the single-crystal structures of compounds **1**, **2**, **7**, and **10** could be determined, PXRD measurements as presented in Figure 2 and Figures SI-8−13 confirm the presence of the principal framework structure in all cases. Interestingly, the respective isomorphous compounds combining NO_3^- ions and the ligands $(H\text{-}Me\text{-}trz\text{-}ia)^{2-}$ and $(H\text{-}3py\text{-}trz\text{-}ia)^{2-}$, as expected by the IRMOF concept, are not obtained. Respective cubic compounds could not be obtained despite systematically testing a large variety of synthesis conditions. Instead, the compounds $^3_\infty[\{Cu_6(\mu_4\text{-}O)(\mu_3\text{-}OH)_2(H\text{-}Me\text{-}trz\text{-}ia)_4\}[Cu(H_2O)_6](NO_3)_2 \cdot 10H_2O$ (**11**) and $^3_\infty[Cu_2(H\text{-}3py\text{-}trz\text{-}ia)_2(H_2O)_3] \cdot 6H_2O \cdot MeCN$ (**12**) are formed. On the basis of these observations, it can be concluded that **1**−**10** follow the IRMOF concept. Unexpectedly, **11** and **12** do not follow up the concept, although they were prepared from the same starting materials and under the same reactions conditions. Whereas the IRMOF concept represents a geometrical approach, kinetics and thermodynamics play an important role in the formation of products, leading to unexpected structures as can be seen from **11** and **12**, which are discussed below. This shows the limitation of the IRMOF concept, which does not take kinetic or thermodynamic aspects into account.

The fact that **1**−**10** are isomorphous, and the triazole is oriented perpendicular with respect to the mirror plane, leads to disorder of the substituents. In case of **9** and **10**, four neighboring pyridine units coordinate to an additional Cu^+ ion Cu3 in a tetrahedral manner, and the counterion is disordered in the pore structure (Figure SI-4).

From the thermogravimetric analyses presented in Figure SI-14, it can be concluded that the thermal decomposition of all

dx.doi.org/10.1021/ic3003228 | *Inorg. Chem.* 2012, 51, 7579−7586

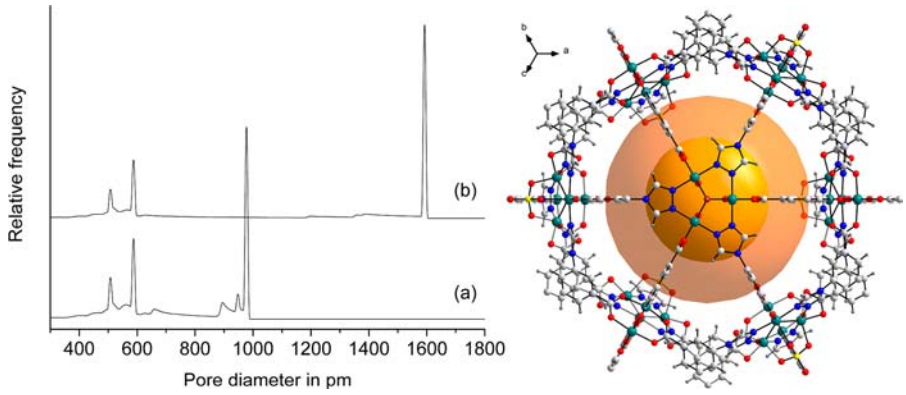

Figure 3. Pore size distribution of **1** (a) with and (b) without sulfate ions (left) and visualization of the spherical pore with sizes of 980 pm with sulfate ions and of 1590 pm without sulfate ions (right).

compounds of the isomorphous MOF **1**−**10** series takes place in the range of 270−300 °C. During the decomposition, carbon dioxide is released from the isophthalate groups of the ligands as evidenced by the recorded mass spectra (Figure SI-14, m/z = 44 $[CO_2]^+$). However, the TD-PXRD studies reveal that the crystallinity of **1**−**5** is lost at 140−170 °C (Figure SI-15), while for **6**−**10** only an intensity reduction is observed (Figure SI-16). Prior to the adsorption studies, all samples were treated by Soxhlet extraction with methanol to achieve a complete solvent exchange. This procedure has previously been shown by other groups to facilitate the activation process significantly.[3,18] In our work, we have successfully applied this technique also to other MOFs.[19,13] In the respective PXRD patterns (Figure 2), the observed intensity deviations correspond to different pore contents.[20−23] During activation in vacuum and sorption experiments, strong changes of the reflection intensities are observed (Figure 2). Upon activation, the intensities of the 110 reflections at 4.8° increase dramatically as compared to the 200, 211, and 220 reflections at 6.8°, 8.4°, and 9.7°, respectively. Notably, the frameworks remain intact as the original states can be fully restored by resolvation of the activated samples with methanol.

PORE SIZE DISTRIBUTION

Figure 3 presents the pore size distribution (PSD) of **1**, which was geometrically determined from the crystal structure.[24] The PSD of **1** (Figure 3a) shows three distinct pore diameters. While the pore diameter of 980 pm can be assigned to the cage of **1** (Figure 3 right), the maxima at smaller pore diameters of 510 and 580 pm belong to the windows between the cavities. The spherical pore in the center of the cage is limited to a size of 980 pm by the van der Waals contacts to the sulfate ions. If the sulfate ions are neglected for determination of the pore size distribution (cf., Figure 3b), a tremendous increase of the largest pore diameter up to 1590 pm is observed. However, the pore diameters, which have to be assigned to the windows, remain unchanged. In contrast to the **rht** MOF[25] $(^3_\infty[Cu_6O(TZI)_3(H_2O)_9(NO_3)\}_3\cdot 15H_2O$, TZI: 5-tetrazolyl-isophthalate), which contains similar building blocks and a bimodal pore size distribution, the herein presented MOF series shows uniform spherical pores resulting from the different topology, that is, connection of the nodal points.

As by the IRMOF concept,[6] it is generally anticipated that the pore diameter can be influenced by the choice of ligands with different sterical demand. Unexpectedly, the calculated PSDs of the isomorphous compounds **2**−**10** (Figure SI-5) show no significant deviations as compared to the PSD of **1** with the unsubstituted ligand $(trz\text{-}ia)^{2-}$. This can be understood by the fact that the substituents on the 1,2,4-triazole ring are not oriented to the center of the cage. On the contrary, they are located near the windows of the cage, blocking them partially.

ADSORPTION STUDIES

Motivated by the calculated porosity of **1**−**10**, which is higher than 50%, comprehensive sorption studies were carried out for

Table 2. Summary of Calculated and Experimental Adsorption Data of 1−10

	$V_{pore,calc}$[17] in %	$\rho_{lattice}$ in g cm^{-3}	$V_{pore,calc}$ in cm^3 g^{-1}	$V_{pore,N2}$[27] in cm^3 g^{-1}	S_{BET}[28] in m^2 g^{-1}	$V_{pore,CO2}$[27] in cm^3 g^{-1}
1	66	0.859	0.76	0.59	1354	0.61
2	65	0.904	0.72	0.55	1256	0.56
3	−[a]	0.904[c]	−[a]	0.54	1197	0.55
4	−[a]	0.917[c]	−[a]	0.52	1274	0.50
5	−[a]	0.947[c]	−[a]			0.40
6	−[a]	1.055[c]	−[a]	0.46	1081	0.50
7	50[b]	1.070	0.47[b]	0.46	1120	0.52
8	−[a]	1.083[c]	−[a]	0.40	944	0.43
9	−[a]	1.122[c]	−[a]	0.43	945	0.48
10	49[b]	1.166	0.42[b]	0.37	857	0.43

[a]The single-crystal structure was not determined. [b]Estimated values taking the disorder of substituents into account. [c]Calculated using lattice constants as indexed from powder diffraction patterns.

N_2 (77 K) and CO_2 (298 K) as adsorptives. The recorded isotherms of all compounds are shown in Figures SI-17−26. All isotherms observed are of type I according to the IUPAC classification of physisorption isotherms.[26] While **1**−**5** show their maximum capacities already after activation in vacuum at room temperature, **6**−**10** can be activated at 100 °C/vacuum. Table 2 summarizes the textural properties of **1**−**10** in comparison with calculated data based on the X-ray crystal structures.

According to the nitrogen and carbon dioxide isotherms, **1** possesses a total pore volume of 0.59 cm^3 g^{-1} for nitrogen (77 K) and 0.61 cm^3 g^{-1} for carbon dioxide (298 K), calculated by applying the Gurvich rule.[27] Both values are lower than the pore volume of 0.76 cm^3 g^{-1} as calculated on the basis of the crystal structure data. At a relative pressure of p/p_0 = 0.05, **1** already reaches 89% of its maximum sorption capacity of V_{STP} = 365 cm^3 g^{-1} (16.3 mmol g^{-1}) for nitrogen (77 K) at p/p_0 = 0.95. This high uptake in the low pressure region of the nitrogen isotherm

dx.doi.org/10.1021/ic3003228 | Inorg. Chem. 2012, 51, 7579−7586

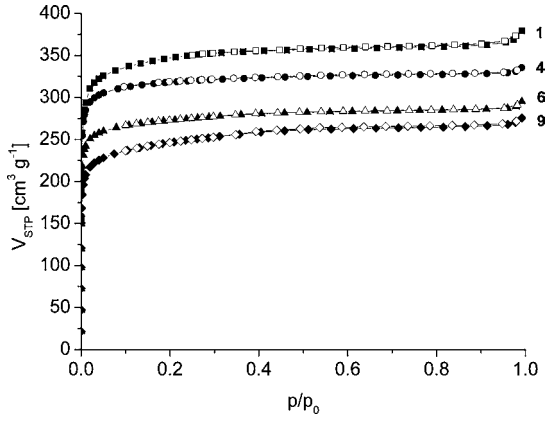

Figure 4. Nitrogen sorption isotherms (77 K, closed symbols adsorption, open symbols desorption; p_0 = 0.0972 MPa) of the sulfate-containing compounds **1**, **4**, **6**, and **9** with varying substituents of increasing sterical demand on the 1,2,4-triazole ring of the ligand.

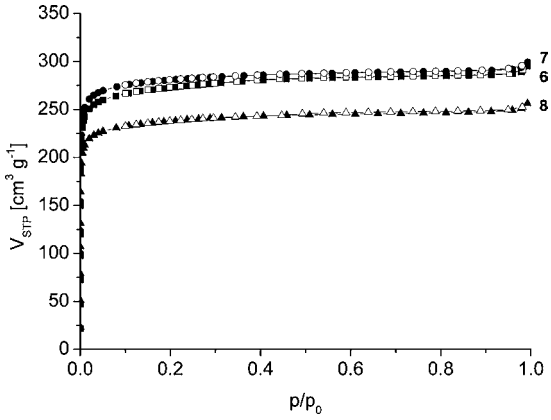

Figure 5. Nitrogen sorption isotherms (77 K, closed symbols adsorption, open symbols desorption; p_0 = 0.0972 MPa) of compounds **6**–**8** varying only in the incorporated counterions.

impressively demonstrates the pronounced microporosity of the MOF. This is also expressed by the specific surface area of S_{BET} = 1354 m^2 g^{-1}.[28] The observed surface area of **1** is even higher than that of the well-known MIL-53 (1190 m^2 g^{-1})[29] and $Cu_3(btc)_2$ (1270 m^2 g^{-1}).[30,31] Besides that, **1** adsorbs a maximum excess amount of 11.72 mmol g^{-1} (2.37 wt %) H_2 at 6.5 MPa (77 K) (Figure SI-27).

The results of the adsorption measurements (Table 2) confirm the expected dependence of the pore volume on the sterical demand of the substituents on the ligand as well as the influence of the incorporated anions. Figure 4 presents the nitrogen adsorption isotherms (77 K) of the sulfate-containing compounds **1**, **4**, **6**, and **9**, which differ only in the substituents R on the ligand (R = H, Me, Ph, 3py). While **1**, containing the unsubstituted triazolyl isophthalate ligand, shows the highest uptake within the isomorphous series **1**–**10**, the additional methyl group (**4**) leads to a significantly lower capacity. Further increase of the sterical demand of the substituent by the phenyl (**6**) and 3-pyridyl groups (**9**) again leads to lower sorption capacities. The difference between **6** and **9** is caused by the additional copper(I) ion incorporated in the framework of **9** and the sulfate counterion in the pore structure. The same tendency is observed within the series **6**, **7**, and **8** (Figure 5), which all contain the phenyl substituted triazolyl isophthalate ligand (H-Ph-trz-ia)$^{2-}$ and different anions. While the sulfate and selenate-containing compounds **6** and **7** differ only slightly in their sorption capacities, a larger decrease is observed for **8**. To equalize the charge balance of the framework, **8** contains eight nitrate ions instead of four sulfate (**6**) or selenate ions (**7**) per formula unit. In this way, the lower observed pore volume can be explained by a partial occupation of the pore by the nitrate ions resulting in a reduced pore volume.

$^3_\infty[Cu_6(\mu_4\text{-}O)(\mu_3\text{-}OH)_2(H\text{-}Metrz\text{-}ia)_4][Cu(H_2O)_6](NO_3)_2\cdot 10H_2O$ (11)

The solvothermal reaction of $Cu(NO_3)_2\cdot 3H_2O$ and H_2(H-Metrz-ia) in H_2O/MeCN (1:1, v/v) leads to the formation of a metal–organic framework, which is not isomorphous to the cubic series **1**–**10**. Instead, the three-dimensional MOF $^3_\infty[Cu_6(\mu_4\text{-}O)(\mu_3\text{-}OH)_2(H\text{-}Metrz\text{-}ia)_4][Cu(H_2O)_6](NO_3)_2\cdot 10H_2O$ (**11**) is obtained. **11** crystallizes in the trigonal space group $R\bar{3}$ (No. 148) with three formula units per unit cell.

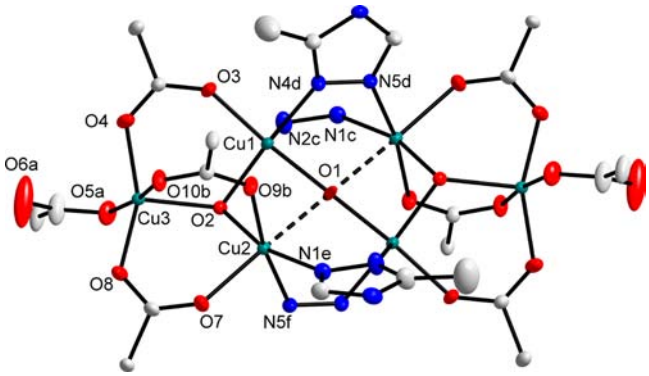

Figure 6. Ellipsoid representation (50% probability) of the hexanuclear structural motif of **11**. Hydrogen atoms are omitted for clarity. Symmetry codes: a, $1-y, x-y, z$; b, $1/3+y, 2/3-x+y, 2/3-z$; c, $1/3+x-y, -1/3+x, 4/3-z$; d, $x-y, x, 1-z$; e, $1/3-x+y, 2/3-x, -1/3+z$; f, $2/3-x+y, 1/3-x, 1/3+z$.

As presented in Figure 6, the structural motif of **11** consists of a hexanuclear $[Cu_6(\mu_4\text{-}O)(\mu_3\text{-}OH)_2]^{8+}$ unit, which is composed of two trinuclear $[Cu_3(\mu_3\text{-}OH)]^{5+}$ subunits that are brigded by a four-connecting O^{2-} anion (O1) as well as by four bidentately binding triazole groups. The two crystallographically independent Cu^{2+} ions Cu1 and Cu2 possess N_2O_4 coordination spheres, whereas Cu3 is coordinated by five oxygen atoms. Selected bond lengths and angles can be found in Table SI-4. While Cu2 is distorted octahedrally and Cu3 square pyramidally coordinated, Cu1 shows a [5 + 1] coordination sphere due to the much weaker interaction Cu1···O9b of 284.4(2).

In contrast, the two remaining carboxylate groups coordinate to the outer Cu^{2+} ions Cu3 in a monodentate fashion. In total, 12 functional groups are coordinating to the hexanuclear $[Cu_6(\mu_4\text{-}O)(\mu_3\text{-}OH)_2]^{8+}$ unit. Hence, this building block represents a 12-connecting nodal point. Together with the (H-Metrz-ia)$^{2-}$ ligands as three-connecting nodal points, the topology of the resulting three-dimensional framework can be described by the unprecedented point symbol $\{4^2\cdot 6\}_4\{4^{24}\cdot 6^{34}\cdot 8^8\}$. For the given point symbol, there is no assignment to a three-letter-code available in the TOPOS&RCSR database.[16] The 12-connecting nodal point represents a novel secondary building unit; no similar $[Cu_6(\mu_4\text{-}O)(\mu_3\text{-}OH)_2]^{8+}$ units with the same connection sequence are described in the literature.

According to Figure 7, it is visible that in the crystallographic *c* direction the network of **11** possesses channels with a diameter of

dx.doi.org/10.1021/ic3003228 | Inorg. Chem. 2012, 51, 7579–7586

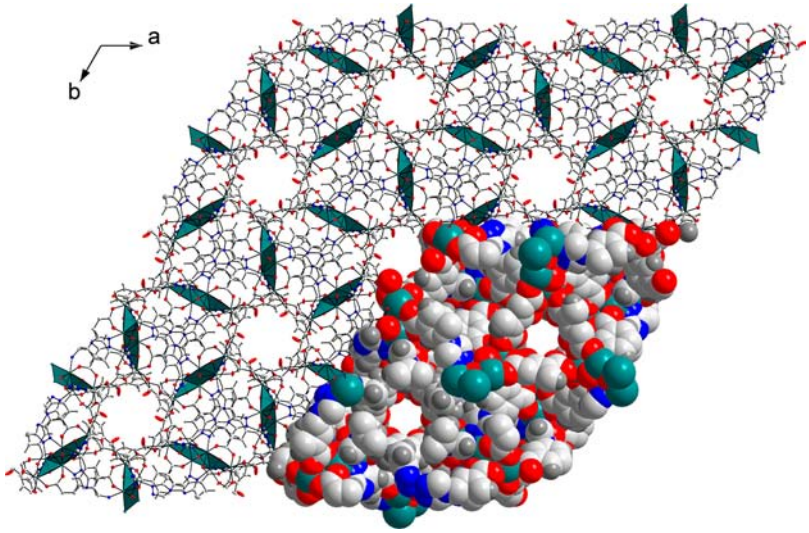

Figure 7. Representation of a 2·2·2 super cell of **11** along the crystallographic *c* direction. The guest molecules in the channels are omitted for clarity.

about 500 pm. After removal of the guest molecules, a solvent-accessible pore volume of 37% can be calculated from crystal structure data.[17]

The positive charge of the hexanuclear $[Cu_6(\mu_4\text{-}O)(\mu_3\text{-}OH)_2]^{8+}$ unit is balanced by four $(H\text{-}Metrz\text{-}ia)^{2-}$ ions, resulting in a neutral network. Nevertheless, besides 10 disordered water molecules, the channels of **11** host a hexaaqua copper(II) complex, whose positive charge is balanced by additional nitrate ions, which are also located in the pore. The Cu^{2+} ion of the $[Cu(H_2O)_6]^{2+}$ complex resides on the $\bar{3}$ position, whereas the aquo ligands reside on general positions. The aquo ligands are found to be disordered on two positions with a refined ratio of 77%:23%, so that with Cu4−O11A 203.40(1) pm and Cu4−O11B 245.36(1) pm there are two different bond lengths. This is expected due to the Jahn−Teller effect resulting in an distorted octahedral coordination with four short and two long bonds. Similar bond lengths are found in the literature.[32,33]

The phase purity of the obtained product is confirmed by X-ray powder diffraction (Figure SI-6, left). Furthermore, the thermal stability of the coordination polymer is assessed by temperature-dependent X-ray powder diffraction (TD-PXRD, Figure SI-6, right) and TG−DTA-MS analysis (Figure SI-7). The TD-PXRD shows that no phase transition occurs up to a temperature of 290 °C. Above 290 °C, the crystallinity of the MOF is lost. In combination with the TG−DTA-MS analysis, decomposition of the framework can be concluded, which proceeds by release of carbon dioxide from the carboxylate groups (m/z = 44 $[CO_2]^+$), water (m/z = 18 $[H_2O]^+$), and acetonitrile (m/z = 41 $[C_2H_3N]^+$) by decomposition of the triazole rings. Below the decomposition temperature, a mass loss of 3.1% between 130 and 200 °C is observed, which corresponds to the water molecules contained in the pores (calcd value for 10 noncoordinating water molecules: 3.8%).

■ $^3_\infty[M_2(H\text{-}3py\text{-}trz\text{-}ia)_2(H_2O)_3]$ (M = Cu (12^{Cu}) AND M = Co (12^{Co}))

While the compounds **1**−**10** are isomorphous, the related reaction between $Cu(NO_3)_2{\cdot}3H_2O$ and $H_2(H\text{-}3py\text{-}trz\text{-}ia)$ leads to $^3_\infty[Cu_2(H\text{-}3py\text{-}trz\text{-}ia)_2(H_2O)_3]{\cdot}6H_2O{\cdot}MeCN$ ($\mathbf{12^{Cu}}$). Single crystals of $\mathbf{12^{Cu}}$ suitable for X-ray crystal structure analysis were prepared using diffusion methods or solvothermal synthesis. The isomorphous cobalt containing coordination polymer $^3_\infty[Co_2(H\text{-}3py\text{-}trz\text{-}ia)_2(H_2O)_3]{\cdot}7H_2O{\cdot}MeCN$ ($\mathbf{12^{Co}}$) can be obtained by the reaction of cobalt nitrate or cobalt sulfate and the respective triazolyl isophthalate in H_2O/MeCN (1:1 v/v) using diffusion methods.

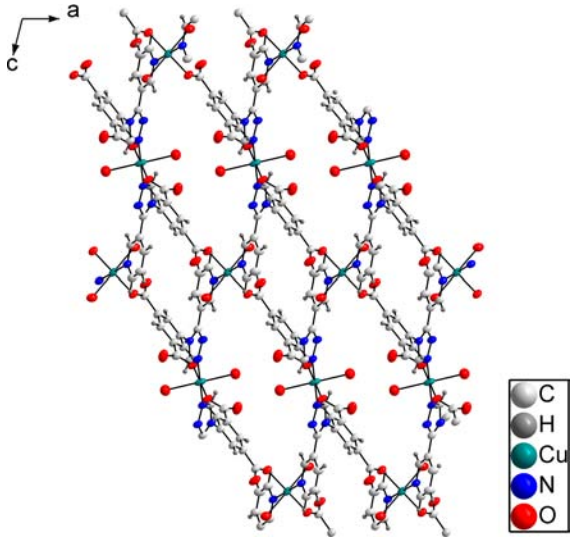

Figure 8. Fragment of the 3D crystal structure of $\mathbf{12^{Cu}}$ with view along [010].

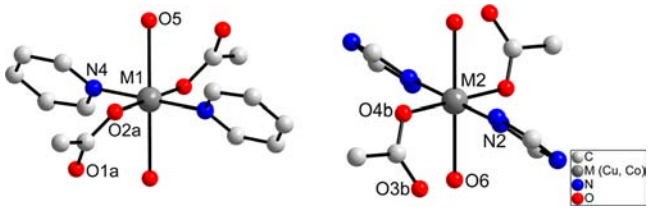

Figure 9. Coordination spheres of the two crystallographically independent metal ions in $\mathbf{12^{Cu}}$ and $\mathbf{12^{Co}}$.

According to the single-crystal X-ray structure analyses, both coordination polymers crystallize in the triclinic space group $P\bar{1}$ (No. 2) with one formula unit per unit cell. The asymmetric unit contains one linker anion and two crystallographically independent metal ions residing on inversion centers (Figure 8). The metal ion M1 is coordinated in an octahedral fashion by

dx.doi.org/10.1021/ic3003228 | Inorg. Chem. 2012, 51, 7579−7586

Table 3. Single-Crystal Structure Data of 1, 2, 7, 10, 11, 12^{Cu}, and 12^{Co}[34]

	1[a]	2[a]	7[a]	10[a]
color and shape	blue block	blue block	blue prism	green prism
crystal dimensions [mm]	0.31 × 0.31 × 0.35	0.22 × 0.23 × 0.24	0.26 × 0.28 × 0.34	0.05 × 0.05 × 0.05
formula	$C_{120}H_{76}N_{36}O_{74}S_4Cu_{18}$	$C_{120}H_{76}N_{36}O_{74}Se_4Cu_{18}$	$C_{192}H_{124}N_{36}O_{74}Se_4Cu_{18}$	$C_{360}H_{224}N_{96}O_{160}Se_{11}Cu_{42}$
M [g mol^{-1}]	4478.12	4665.72	5578.83	11 991.59
temperature [K]	100(2)	100(2)	180(2)	180(2)
diffractometer	STOE IPDS-2T	STOE IPDS-2T	STOE IPDS-2T	BL 14.2 (BESSY-II)[35]
wavelength in pm	71.073	71.073	71.073	82.567
crystal system	cubic	cubic	cubic	cubic
space group	$I\bar{4}3m$ (No. 217)	$I\bar{4}3m$ (No. 217)	$I\bar{4}3m$ (No. 217)	$I\bar{4}3m$ (No. 217)
unit cell [pm/deg]	a = 2586.6(1)	a = 2578.8(2)	a = 2586.7(3)	a = 2575(2)
volume [10^6 pm^3]	17 305(2)	17 149(2)	17 308(3)	17 076(18)
Z	2	2	2	1
density [g cm^{-3}]	0.859	0.904	1.070	1.166
μ(Mo K$_\alpha$) [mm^{-1}]	1.155	1.565	1.561	1.927
$\theta_{min} - \theta_{max}$ [deg]	1.04−25.00	0.96−25.00	1.04−25.00	1.30−29.41
reflections measured	11 239	7345	7170	8093
independent reflections	2793	2424	1725	1580
observed reflections ($I > 2\sigma(I)$)	2483	2173	1647	1411
R_{int}	0.0270	0.0257	0.0690	0.0601
parameters refined	128	129	136	142
R_1 ($I > 2\sigma(I)$)	0.0364	0.0364	0.0779	0.0665
wR_2 (all data)	0.0942	0.0968	0.2168	0.2163
absolute structure parameter	0.54(2)[b]	0.29(2)[b]	0.35(5)[b]	0.48(6)[b]
extinction coefficient		0.00046(6)		
max/min peak [10^{-6} pm^{-3}]	0.7/−0.3	0.3/−0.4	0.9/−0.6	1.4/−1.2

	11	12^{Cu}	12^{Co}
color and shape	green prism	blue prism	purple prism
crystal dimensions [mm]	0.15 × 0.15 × 0.15	0.11 × 0.28 × 0.31	0.12 × 0.23 × 0.40
formula	$C_{132}H_{118}N_{38}O_{81}Cu_{19}$	$C_{16}H_{18.50}N_{4.50}O_{8.50}Cu$	$C_{16}H_{20.50}N_{4.50}O_{9.50}Co$
M [g mol^{-1}]	4739.90	473.39	486.80
temperature [K]	180(2)	180(2)	180(2)
diffractometer	STOE IPDS-I	STOE IPDS-2T	STOE IPDS-2T
wavelength in pm	71.073	71.073	71.073
crystal system	trigonal	triclinic	triclinic
space group	$R\bar{3}$ (No. 148)	$P\bar{1}$ (No. 2)	$P\bar{1}$ (No. 2)
unit cell [pm/deg]	a = 3221.7(2)	a = 782.9(1)	a = 802.31(9)
	c = 1699.05(8)	b = 936.2(1)	b = 953.0(1)
		c = 1514.7(2)	c = 1547.1(2)
		α = 94.70(1)	α = 96.709(9)
		β = 102.89(1)	β = 103.637(9)
		γ = 101.23(1)	γ = 99.063(9)
volume [10^6 pm^3]	15 273(1)	1052.3(2)	1120.6(2)
Z	3	2	2
density [g cm^{-3}]	1.546	1.494	1.443
μ(Mo K$_\alpha$) [mm^{-1}]	2.031	1.091	0.822
$\theta_{min} - \theta_{max}$ [deg]	1.9−28.0	1.0−25.0	1.0−25.0
reflections measured	21 889	6546	7110
independent reflections	8019	3596	3808
observed reflections ($I > 2\sigma(I)$)	6107	2970	3372
R_{int}	0.0294	0.0407	0.0190
Pparameters refined	420	279	295
R_1 ($I > 2\sigma(I)$)	0.0514	0.0547	0.0533
wR_2 (all data)	0.1599	0.1752	0.1764
extinction coefficient			0.043(6)
max/min peak [10^{-6} pm^{-3}]	3.4/−2.4	1.1/−0.6	1.4/−0.5

[a]The PLATON/SQUEEZE[17,20] routine was used to remove the diffuse residual electron density as no solvent molecules could be detected during single-crystal structure refinement. [b]Inversion twinning refined during crystal structure analysis.

two monodentate carboxylates, two pyridine functions, and two water molecules in trans position, whereas the coordination sphere of M2 is built up by two monodentate carboxylates, two triazole groups, and two water molecules forming a distorted

dx.doi.org/10.1021/ic3003228 | Inorg. Chem. 2012, 51, 7579−7586

octahedron (Figure 9). Selected bond lengths and angles can be found in Table SI-5. In comparison to $\mathbf{12}^{Co}$, the octahedral coordination sphere of $\mathbf{12}^{Cu}$ is more elongated due to the Jahn–Teller effect.

Both metal ions in $\mathbf{12}^{Cu}$ and $\mathbf{12}^{Co}$ represent planar 4-fold nodal points, and the ligands act as tetradentate linkers in a 3D network with **pts** topology.[16] With narrow pore channels of about 200–250 pm in crystallographic *b* direction (Figure 8), the structures possess a calculated porosity of 29% in case of $\mathbf{12}^{Cu}$ and 31% in case of $\mathbf{12}^{Co}$ according to PLATON.[17]

CONCLUSIONS

Following the IRMOF concept, we have presented a series of 10 isomorphous cubic MOFs **1**-**10** with **twf-d** topology and a thermal stability up to 300 °C as evidenced by TG–MS analyses. In closely related reactions, the compounds **11** and **12** are formed, which have compositions and structures different from those of **1**–**10** (Table 3). This points out that small changes in starting materials or reaction conditions can lead to reaction products with completely different structures. Kinetic and thermodynamic aspects are very important, but are not taken into account in the concept of isoreticular MOFs, which is a geometrical approach. All compounds of the isomorphous series are easily accessible in multigram scale syntheses, facilitating future applications. We are currently investigating the catalytic activity of these compounds in standard test reactions. The pronounced microporosity is evidenced by adsorption measurements resulting in a maximum pore volume of up to 0.59 $cm^3\ g^{-1}$ for N_2 for **1** at 77 K and specific surfaces up to $S_{BET} = 1354\ m^2\ g^{-1}$. While variation of the sterical demand of the substituents in the 3-position of the 1,2,4-triazole as well as different counterions modify the pore volumes to 0.37–0.59 $cm^3\ g^{-1}$, the diameters of the spherical pores remain unchanged. By choice of the anion–ligand combination, fine-tuning of the pore volume can easily be achieved. On the basis of these results, we are currently investigating the applicability of these compounds for gas separation processes.

ASSOCIATED CONTENT

Supporting Information

Experimental details for ligand and MOF syntheses, detailed characterization by IR spectroscopy, X-ray diffraction, and TG/DTA-MS methods, by adsorption measurements, as well as by temperature-dependent magnetic susceptibility measurement. This material is available free of charge via the Internet at http://pubs.acs.org. CCDC 854984–854994 contain the supplementary crystallographic data. These data can be obtained free of charge from the Cambridge Crystallographic Data Centre via www.ccdc.cam.ac.uk/data_request/cif.

AUTHOR INFORMATION

Corresponding Author

*E-mail: krautscheid@rz.uni-leipzig.de.

Notes

The authors declare no competing financial interest.

ACKNOWLEDGMENTS

We thank M.Sc. F. Kettner for assistance with TG–MS analyses, Prof. B. Kersting and M.Sc. F. Schleife for magnetic susceptibility data, and Dipl.-Ing. E. Altmann for sample preparation. Financial support by Deutsche Forschungsgemeinschaft (DFG SPP 1362 - Poröse metallorganische Gerüstverbindungen, KR 1675/7-1 and STA 428/17-1), the University of Leipzig (PbF-1), and the graduate school BuildMoNa is gratefully acknowledged. D.L. acknowledges the fellowship of the Fonds der Chemischen Industrie. J.L. and M.H. are grateful for ESF fellowships. This work was funded by the European Union and the Free State of Saxony. The Helmholtz-Zentrum Berlin (BESSY-II) is acknowledged for granting beamtime and travel support, in particular Dr. U. Müller and his team for assistance during data collection. Diffraction data have been collected on BL14.2 operated by the Joint Berlin MX-Laboratory at the BESSY II electron storage ring (Berlin-Adlershof, Germany).

DEDICATION

This work is dedicated to Prof. Dr. Horst Hennig on the occasion of his 75th birthday.

REFERENCES

(1) Janiak, C.; Vieth, J. K. *New J. Chem.* **2010**, *34*, 2366–2388.
(2) (a) Alessandro, D. M. D.; Smit, B.; Long, J. R. *Angew. Chem.* **2010**, *122*, 6194–6219; *Angew. Chem., Int. Ed.* **2010**, *49*, 6058–6082. (b) Debatin, F.; Thomas, A.; Kelling, A.; Hedin, N.; Bacsik, Z.; Senkovska, I.; Kaskel, S.; Junginger, M.; Müller, H.; Schilde, U.; Jäger, C.; Friedrich, A.; Holdt, H.-J. *Angew. Chem.* **2010**, *122*, 1280–1284; *Angew. Chem., Int. Ed.* **2010**, *49*, 1258–1262.
(3) Hartmann, M.; Kunz, S.; Himsl, D.; Tangermann, O.; Ernst, S.; Wagener, A. *Langmuir* **2008**, *24*, 8634–8642.
(4) (a) Bauer, C. A.; Timofeeva, T. V.; Settersten, T. B.; Patterson, B. D.; Liu, V. H.; Simmons, B. A.; Allendorf, M. D. *J. Am. Chem. Soc.* **2007**, *129*, 7136–7144. (b) Harbuzaru, B. V.; Corma, A.; Rey, F.; Atienzar, P.; Jordá, J. L.; García, H.; Ananias, D.; Carlos, L. D.; Rocha, J. *Angew. Chem.* **2008**, *120*, 1096–1099; *Angew. Chem., Int. Ed.* **2008**, *47*, 1080–1083.
(5) Corma, A.; García, H.; Llabres i Xamena, F. X. *Chem. Rev.* **2010**, *110*, 4606–4655.
(6) Eddaoudi, M.; Kim, J.; Rosi, N.; Vodak, D.; Wachter, J.; O'Keeffe, M.; Yaghi, O. M. *Science* **2002**, *295*, 469–472.
(7) Wilmer, C. E.; Leaf, M.; Lee, C. Y.; Farha, O. K.; Hauser, B. G.; Hupp, J. T.; Snurr, R. Q. *Nat. Chem.* **2012**, *4*, 83–89.
(8) Banerjee, R.; Phan, A.; Wang, B.; Knobler, C.; Furukawa, H.; O'Keeffe, M.; Yaghi, O. M. *Science* **2008**, *319*, 939–943.
(9) (a) Ponomarova, V.; Komarchuk, V. V.; Boldog, I.; Chernega, A. N.; Sieler, J.; Domasevitch, K. V. *Chem. Commun.* **2002**, 436–437. (b) Hunger, J.; Krautscheid, H.; Sieler, J. *Cryst. Growth Des.* **2009**, *9*, 4613–4625.
(10) (a) Engelfriet, D. W.; Den Brinker, W.; Verschoor, G. C.; Gorter, S. *Acta Crystallogr.* **1979**, *B35*, 2922–2927. (b) Garcia, Y.; van Koningsbruggen, P. J.; Kooijman, H.; Spek, A. L.; Haasnoot, J. G.; Kahn, O. *Eur. J. Inorg. Chem.* **2000**, 307–314. (c) Haasnoot, J. G. *Coord. Chem. Rev.* **2000**, *200–202*, 131–185. (d) Beckmann, U.; Brooker, S. *Coord. Chem. Rev.* **2003**, *245*, 17–29. (e) Klingele, M. H.; Brooker, S. *Coord. Chem. Rev.* **2003**, *241*, 119–132. (f) Lysenko, A. B.; Govor, E. V.; Krautscheid, H.; Domasevitch, K. V. *Dalton Trans.* **2006**, 3772–3776. (g) Habib, H. A.; Sanchiz, J.; Janiak, C. *Dalton Trans.* **2008**, 1742–1751. (h) Huang, X.-C.; Luo, W.; Shen, Y.-F.; Lin, X.-J.; Li, D. *Chem. Commun.* **2008**, 3995–3997. (i) Habib, H. A.; Hoffmann, A.; Höppe, H. A.; Steinfeld, G.; Janiak, C. *Inorg. Chem.* **2009**, *48*, 2166–2180.
(11) Aromi, G.; Barrios, L. A.; Roubeau, O.; Gamez, P. *Coord. Chem. Rev.* **2011**, *255*, 485–546.
(12) (a) Dinča, M.; Liu, A. F.; Long, J. R. *J. Am. Chem. Soc.* **2006**, *128*, 8904–8913. (b) Dinča, M.; Dailly, A.; Liu, Y.; Brown, C. M.; Neumann, D. A.; Long, J. R. *J. Am. Chem. Soc.* **2006**, *128*, 16876–16883.
(13) Lässig, D.; Lincke, J.; Moellmer, J.; Reichenbach, C.; Moeller, A.; Gläser, R.; Kalies, G.; Cychosz, K. A.; Thommes, M.; Staudt, R.; Krautscheid, H. *Angew. Chem.* **2011**, *123*, 10528–10532; *Angew. Chem., Int. Ed.* **2011**, *50*, 10344–10348.
(14) Möllmer, J.; Lange, M.; Möller, A.; Patzschke, C.; Stein, K.; Lässig, D.; Lincke, J.; Gläser, R.; Krautscheid, H.; Staudt, R. *J. Mater. Chem.* **2012**, *22*, 10274–10286.

(15) Lässig, D.; Lincke, J.; Krautscheid, H. *Tetrahedron Lett.* **2010**, *51*, 653−656.
(16) TOPOS 4.0; Blatov, V. A. *IUCr CompComm Newsletter* **2006**, *7*, 4−8; http://www.topos.ssu.samara.ru.
(17) PLATON; Spek, A. L. *J. Appl. Crystallogr.* **2003**, *36*, 7−13.
(18) (a) Roswell, J. L. C.; Yaghi, O. M. *J. Am. Chem. Soc.* **2006**, *128*, 1304−1315. (b) Liu, J.; Culp, J. T.; Natesakhawat, S.; Bockrath, B. C.; Zande, B.; Sankar, S. G.; Garberoglio, G.; Johnson, J. K. *J. Phys. Chem. C* **2007**, *111*, 9305−9313.
(19) (a) Lincke, J.; Lässig, D.; Moellmer, J.; Reichenbach, C.; Puls, A.; Moeller, A.; Gläser, R.; Kalies, G.; Staudt, R.; Krautscheid, H. *Microporous Mesoporous Mater.* **2011**, *142*, 62−69. (b) Reichenbach, C.; Kalies, G.; Lincke, J.; Lässig, D.; Krautscheid, H.; Moellmer, J.; Thommes, M. *Microporous Mesoporous Mater.* **2011**, *142*, 592−600.
(20) van der Sluis, P.; Spek, A. L. *Acta Crystallogr.* **1990**, *A46*, 194−201.
(21) Schlichte, K.; Kratzke, T.; Kaskel, S. *Microporous Mesoporous Mater.* **2004**, *73*, 81−88.
(22) Hafizovic, J.; Bjørgen, M.; Olsbye, U.; Dietzel, P. D. C.; Bordiga, S.; Prestipino, C.; Lamberti, C.; Lillerud, K. P. *J. Am. Chem. Soc.* **2007**, *129*, 3612−3620.
(23) Lincke, J.; Lässig, D.; Stein, K.; Moellmer, J.; Kuttatheyil, A. V.; Reichenbach, C.; Moeller, A.; Staudt, R.; Kalies, G.; Bertmer, M.; Krautscheid, H. *Dalton Trans.* **2012**, *41*, 817−824.
(24) (a) Gelb, L. D.; Gubbins, K. E. *Langmuir* **1999**, *15*, 305−308. (b) Bhattacharya, S.; Gubbins, K. E. *Langmuir* **2006**, *22*, 7726−7731. (c) PSDsolv ; Bhattacharya, S.; http://supriyo.net/research/psd/psd.htm.
(25) Nouar, F.; Eubank, J. F.; Bousquet, T.; Wojtas, L.; Zaworotko, M. J.; Eddaoudi, M. *J. Am. Chem. Soc.* **2008**, *130*, 1833−1835.
(26) Sing, K. S. W.; Everett, D. H.; Haul, R. A. W.; Mouscou, L.; Pierotti, R. A.; Rouquerol, J.; Siemieniewska, T. *Pure Appl. Chem.* **1985**, *57*, 603−619.
(27) Gurvich, L. *J. Phys. Chem. Soc. Russ.* **1915**, *47*, 805−827.
(28) Moellmer, J.; Celer, E. B.; Luebke, R.; Cairns, A. J.; Staudt, R.; Eddaoudi, M.; Thommes, M. *Microporous Mesoporous Mater.* **2010**, *12*, 345−353.
(29) Loiseau, T.; Serre, C.; Huguenard, C.; Fink, G.; Taulelle, F.; Henry, M.; Bataille, T.; Férey, G. *Chem.-Eur. J.* **2004**, *10*, 1373−1382.
(30) Chui, S. S.-Y.; Lo, S. M.-F.; Charmant, J. P. H.; Orpen, A. G.; Williams, I. D. *Science* **1999**, *283*, 1148−1150.
(31) Möllmer, J.; Möller, A.; Dreisbach, F.; Gläser, R.; Staudt, R. *Microporous Mesoporous Mater.* **2011**, *138*, 140−148.
(32) Muesmann, T. W. T.; Zitzer, C.; Mietrach, A.; Klüner, T.; Christoffers, J.; Wickleder, M. S. *Dalton Trans.* **2011**, *40*, 3128−3141.
(33) Couldwell, C.; Prout, K.; Robey, D.; Taylor, R. *Acta Crystallogr.* **1978**, *B34*, 1491−1499.
(34) Sheldrick, G. M. *Acta Crystallogr.* **2008**, *A64*, 112−122.
(35) Mueller, U.; Darowski, N.; Fuchs, M. R.; Förster, R.; Hellmig, M.; Paithankar, K. S.; Pühringer, S.; Steffien, M.; Zocher, G.; Weiss, M. S. *J. Synchrotron Radat.* **2012**, *19*, 442−449.